Solar Phys (2016) 291:2243–2252
DOI 10.1007/s11207-016-0984-0

Spectropolarimetry of Atomic and Molecular Lines near 4135 nm

Matthew James Penn[1] · Han Uitenbroek[2] · Alan Clark[3] · Roy Coulter[4] · Phil Goode[4] · Wenda Cao[4]

Received: 15 October 2015 / Accepted: 24 August 2016 / Published online: 9 September 2016
© Springer Science+Business Media Dordrecht 2016

Abstract New spatially scanned spectropolarimetry sunspot observations are made of photospheric atomic and molecular absorption lines near 4135 nm. The relative splittings among several atomic lines are measured and shown to agree with values calculated with configuration interaction and intermediate coupling. Large splitting is seen in a line identified with Fe I at 4137 nm, showing multiple Stokes V components and an unusual linear polarization. This line will be a sensitive probe of quiet-Sun magnetic fields, with a magnetic sensitivity of 2.5 times higher than that of the well-known 1565 nm Fe I line.

Keywords Solar magnetic fields · Solar atmosphere · Detectors

1. Introduction

Measurements of solar magnetic fields are essential to modern research efforts. Newly built telescopes and their instruments (*i.e.* the *New Solar Telescope* and the *Cryogenic Infrared Spectrograph*, Cao *et al.*, 2010) and telescopes and instruments currently under construction (*i.e.* the *Daniel K. Inyouye Solar Telescope* and the *Cryogenic Near-IR Spectro-Polarimeter*, Lin, 2003) have new infrared magnetic observations in their core science programs. Historically, measurements of magnetic fields at infrared wavelengths have enabled new scientific advances in solar physics; these instruments intend to capitalize on such observations and seek new infrared tools as well. It is well known that for solar spectral lines with identical magnetic splitting, the relative sensitivity of lines to solar magnetic fields increases with increasing wavelength. As a method to determine which spectral lines to target for increased

✉ M.J. Penn
mpenn@nso.edu

1 National Solar Observatory, 950 N Cherry Av., Tucson, AZ 85726, USA

2 National Solar Observatory, Sunspot, NM 88349, USA

3 Dept. of Physics and Astronomy, University of Calgary, Science B 605, 2500 University Dr NW, Calgary, AB T2N 1N4, Canada

4 Big Bear Solar Observatory, 40386 N Shore Ln, Big Bear, CA 92314, USA

accuracy in measuring the solar magnetic field, the concept of the magnetic resolution of a spectral line can be used. The magnetic sensitivity is determined by the ratio of the magnetic Zeeman splitting [$\lambda^2 g_{\rm eff}$] and the Doppler line broadening [λ] and thus varies as $\lambda g_{\rm eff}$. The most sensitive probes of the solar magnetic field currently include the Fe I 1564.8 nm spectral line ($\lambda g_{\rm eff} = 4695$) for photospheric fields, the Ti I 2233 nm line ($\lambda g_{\rm eff} = 5778$) for fields in cold sunspot umbrae, and the Mg I 12 381 nm line ($\lambda g_{\rm eff} = 12\,318$) for penumbral and plage magnetic fields. Reports of other very sensitive spectral lines near 4135 nm have been made, but no measurements have been published.

Identification of infrared lines is still a challenging task, and several lines remain unidentified even today (Geller, 1995). From laboratory work, lines from high-energy transitions in Fe I (in particular from the $3d^6 4s6s$ to $3d^6 4s6p$ configurations) have "... fragmented analysis with only a few lines known." (Johansson and Cowley, 1988). For lines in the 4135 nm region, only one identification is given by Nave *et al.* (1994) for the 4136.4908 nm line. The energy levels for the transition correspond to 56 541.592 $\rm cm^{-1}$ and 54 124.740 $\rm cm^{-1}$ for the upper and lower levels, respectively, producing a transition at 2416.86 $\rm cm^{-1}$ or 4136.48579 nm. The electronic configurations and terms listed by Nave *et al.* (1994) are $3d^6 4s(^6D)6p(^7P^0)$ and $3d^6 4s(^6D)6s(g^7D)$ for the upper and lower levels. Spin-orbit (LS) coupling (*e.g.* Beckers, 1969) suggests the magnetic sensitivity of this transition gives $g_{\rm eff} = 1.70$.

Using theoretical models and fitting to laboratory spectra, Kurucz (2011) has published a set of infrared line identifications with electron configurations and terms for the upper and lower levels for these lines, as well as the Landé-g values for the levels of the lines from Fe I (Kurucz, 2011). These calculations differ from previous work in that the energy levels are not specifically assigned to an individual electronic configuration and term, but rather to a superposition of overlapping configurations. These configuration interactions are solved to produce an eigenvector of electronic states with a set of contribution coefficients for each state. The energy level is then composed of the sum of these individual levels. With a mixture of electronic configurations for the upper and lower states of the 4136.5 nm transition, LS coupling is applied to each possible combination of upper and lower states weighted with the proper coefficients to produce a value for the magnetic sensitivity of the spectral line; this calculation is called intermediate coupling. For the Fe I 4136.5 nm line the computed value for intermediate coupling is $g_{\rm eff} = 1.62$. While intermediate coupling gives a similar value to LS coupling in this example, this is not always the case.

To determine the relative importance of mixed terms for the energy levels that produce a particular spectral line, the Zeeman splittings of spectral lines measured in the laboratory can be compared against the predictions from both LS and intermediate coupling (Curtis, 2003). The observations presented in this work provide the first such experimental data for the Sun, which can be used to address such questions about several spectral lines near 4135 nm. Furthermore, the polarized spectral line profiles observed in sunspots and presented in this article will provide an experimental constraint on the intermediate coupling theory used to compute the Landé-g values. While the values of $g_{\rm eff}$ have been computed for intermediate coupling, the polarized spectral line profiles themselves have not been computed. These profiles are critical when these spectral lines are used to infer the magnetic fields on the Sun. They can be obtained by first computing the expected LS coupling Zeeman patterns for all the configuration interaction levels, and then weighting these patterns with the proper coefficients.

In Section 2 we review the atomic levels of the relevant atomic and molecular lines near 4135 nm, in Section 3 we discuss new solar observations of this part of the spectrum, and in Section 4 we present the wavelengths and magnetic splittings measured for these lines.

2. Lines near 4135 nm

Observations of the quiet-Sun photospheric spectrum near 4135 nm were made from space with the *Atmospheric Trace Molecular Spectroscopic Experiment* (ATMOS) (Farmer and Norton, 1989) and from the ground at the National Solar Observatory's (NSO) *McMath/Pierce Solar Facility* (McM/P) (Wallace and Livingston, 2003). Observations of the sunspot umbral spectrum near 4135 nm were also made at the McM/P (Wallace, Hinkle, and Livingston, 2002; Wallace and Livingston, 1992). Line identifications are given in the McM/P spectra and have also been made for the ATMOS spectra (Geller, 1992).

Table 1 lists the observed atomic spectral lines in this part of the solar spectrum as seen in the quiet-Sun photosphere. Here the first wavelength values (with the K subscript) are taken from Kurucz (2011), as are the values for $\log(gf)$ (*i.e.* the logarithm of the weighted oscillator strength). The second wavelength values and the line depth values (with the G subscript) are taken from Geller (1992), for this case the line depths have been converted to continuum percentages. Finally, the last two columns (with the NAC subscript) represent recent observations taken from the McM/P, which are described in more detail in the following section.

The infrared solar spectrum has few atomic lines, and the lines that are present are often weak. To produce lines at these wavelengths, the energy difference between the upper and lower levels must be small. The energy difference between levels near the ground state of most atoms is larger, resulting in lines in the ultraviolet (UV) or visible. Only at higher excited states are upper and lower levels relatively closely space in energy, and these produce spectral features in the infrared. For both Fe I and Si I, the upper and lower energy levels are rather close to the ionization energies, which are about 63 737 cm^{-1} for Fe I (Sugar and Corliss, 1985) and 65 748 cm^{-1} for Si I (Martin and Zalubas, 1983). As the temperature of the solar plasma drops from the value in the quiet Sun to lower values in sunspots, the electron populations in these energy levels are much lower. For this reason, the strength of these absorption lines is greatly reduced in sunspots, and these spectral lines are not useful tools for examining the physical conditions in sunspot umbrae. In the penumbrae of sunspots, it is expected that the lines probe the physical conditions in the hotter plasma or in brighter penumbral structures. It is expected that these spectral lines will prove most useful as diagnostics for the quiet-Sun plasma.

Table 2 lists the energy levels for each of these lines and the primary level configurations for each level (although it is important to remember that other configurations are important under the condition of configuration interaction). The identifications are taken from Geller (1992) and Wallace and Livingston (2003), with the exception of the 4137 nm line, which is associated with an Fe I transition listed by Kurucz (2011). Electron configuration and terms for Si I were taken from Martin and Zalubas (1983); these authors reported mixing percentages for configuration interactions in the energy levels at 54 871, 56 690, and 58 893 cm^{-1}.

Table 1 Atomic spectral lines.

Species	λ_K [nm]	$\log(gf)$	λ_G [nm]	Depth_G	λ_{NAC} [nm]	Depth_{NAC}
Si I	4122.8421	−2.190	4122.79	3.2	4122.90	0.6
Si I	4132.7169	0.250	4132.72	16.0	4132.75	5.2
Fe I	4136.4857	0.512	4136.47	7.9	4136.50	2.7
Fe I	4137.0095	−1.630	4136.97	3.1	4136.99	0.8
Fe I	4139.2294	0.448	4139.18	6.8	4139.19	2.6
Si I	4142.5516	0.580	4142.47	9.6	4142.48	5.2

Table 2 Line identifications.

Species	λ_K [nm]	Level energy [cm^{-1}]	Level configuration (primary)	Level g_K
Si I	4122.8421	54 871.031	$3s^2 3p5s\,^1P^0$	
		57 295.881	$3s^2 3p5p\,^3P$	
Si I	4132.7169	56 690.903	$3s^2 3p4d\,^3P^0$	
		59 109.959	$3s^2 3p(^2P^0_{3/2})4f\,^2[5/2]$	
Fe I	4136.4857	54 124.740	$3d^6 4s(^6D)6s\ g^7D$	1.650
		56 541.592	$3d^6 4s(^6D)6p\,^7P^0$	1.587
Fe I	4137.0095	54 747.594	$3d^6 4s(^6D)6s\ g^7D$	2.999
		57 164.140	$3d^6 4s(^6D)6p\,^7D^0$	2.642
Fe I	4139.2294	54 611.706	$3d^6 4s(^6D)6s\ g^7D$	1.997
		57 026.956	$3d^6 4s(^6D)6p\,^7F^0$	1.659
Si I	4142.516	58 893.400	$3s^2 3p4d\,^1F^0$	
		61 306.713	$3s^2 3p(^2P^0_{1/2})5f\,^2[7/2]$	

For Fe I, the configurations and terms were taken from Nave *et al.* (1994). For these primary configurations, the values for the L, S, and J quantum numbers are listed, along with the Landé-g value (from Kurucz, 2011) for the energy levels.

For the case of LS coupling, the Landé-g value for the energy level can be given with the well-known expression (*e.g.* Beckers, 1969, Equation 1); then, the value for $g_{\rm eff}$ for the spectral line can be computed from the values for the upper and lower levels as (Beckers, 1969, Equation 6) $g_{\rm eff} = \frac{1}{8}(J_{\rm u} - J_{\rm l})(J_{\rm u} + J_{\rm l} + 1.0)(g_{\rm u}^2 - g_{\rm l}^2)$.

The molecular lines in this region of the spectrum are dominated by OH and SiO lines. Geller (1992) listed several OH lines in this part of the spectrum as observed from the ATMOS data at wavelengths of 4133.26, 4135.10, 4136.79, and 4142.69 nm. In this spectral region, Wallace, Hinkle, and Livingston (2002) identified about 30 lines from SiO and three lines from CO. They also identified seven OH lines, including all of the OH lines from Geller (1992) plus new identifications at roughly 4136.5, 4137.9, and 4139.2 nm.

3. Observations and Data Analysis

Two sets of observations were used to investigate these spectral lines, both taken at the 1.6 m diameter McM/P main telescope and main spectrograph (Pierce, 1964), but using two different instruments. The first measurements were taken with the *Near Infrared Magnetograph* (NIM) instrument (Rabin *et al.*, 1992); the intensity profiles were measured across several sunspots in the late 1990s. The more recent measurements were taken using the *NSO Array Camera* (NAC) with a 1024 × 1024 InSb Alladin 3 array as the detector. While the NIM observations include several additional lines of interest, including lines at 4056 and 4122.8 nm, and were the inspiration for the recent NAC observations, here only the NAC observations are discussed. In a future work more details of the NIM observations will be presented.

In the NAC observations, the wavelength selection in the dewar was made using a one-inch round cold filter (at roughly 60 K) with an 18 nm bandpass centered on 4137 nm with a peak transmission of 75 %. Since the main spectrograph is warm, the observations contain a high background level. Exposure times were 25 microseconds. The McM/P optics

Table 3 McM/P observations.

Number	Date	Time [UT]	Wavelength [nm]	Sunspot	Stokes type
1	02 May 2013	21:08	4120 – 4145	NOAO 11777	I
2	09 Sep 2013	21:10	4136 – 4139	NOAO 11836	I, V
3		21:22	4132 – 4136	NOAO 11837	I, V
4		21:29	4136 – 4139	NOAO 11838	I, V
5	12 Sep 2013	17:07	4136 – 4139	NOAO 11841	I, Q, U, V
6	25 Sep 2013	18:31	4136 – 4139	NOAO 11846	I, Q, U, V

are expected to produce a very small instrumental polarization at this wavelength, and the polarization crosstalk cannot be measured with this dataset.

The polarization analysis for the NAC observations was made using optics positioned at the spectrograph exit port. A reimaging bench using two CaF2 lenses collimated the spectrograph exit and reimaged it onto the NAC detector. A rotating waveplate was positioned at the spectrograph exit focal plane and a linear polarizer was used in the collimated beam. Since the rotating waveplate is positioned near an image plane, deflection of the beam is not an issue, but dust and other transmission features on the waveplate are challenging to remove during calibration. A slow-chopping method was used by rotating the waveplate between exposures. For sunspot scans, a scanning mirror stepped the solar image perpendicular to the spectrograph slit at the end of a sequence of polarization exposures. Background and flat-field corrections were made for each exposure at the waveplate positions. The waveplate rotation positions were calibrated using a second linear polarizer in the beam. Table 3 lists details of the NAC observations.

Because the McM/P adaptive optics system was not used for these observations, the solar pointing of different waveplate sequences is not stable. Only exposures where two or more spectral lines are simultaneously measured were used to compute the relative splitting ratios between lines; in this way, the magnetic fields sampled by the different lines are identical and the different splittings represent the inherently different responses from the spectral lines. The NAC exposure times and the waveplate rotation were run in open-loop mode, resulting in some overhead time where photons were not collected.

4. The Intensity and Polarization Spectra

4.1. Intensity Spectra at 4120 – 4145 nm

The four strongest lines in this spectral region are two each from Fe I and Si I. There are also two weaker lines, one each from Fe I and Si I, and several telluric absorption lines. The spectra are shown in Figure 1. By averaging NAC spectra from many pixels, we were able to produce an average spectrum that has a signal-to-noise ratio about ten times better than in the spectrum used by Wallace and Livingston (2003), but the lines appear weaker in the NAC spectrum because the spectral resolution is lower than that achieved by Wallace and Livingston (2003). Many frames were stitched together to produce this spectrum, where each single NAC image covers about 4 nm of the solar spectrum.

These data were wavelength calibrated using a set of six telluric absorption lines located at 4131.79, 4133.15, 4134.69, 4137.94, 4141.03, and 4144.12 nm as measured in the atlas of Wallace and Livingston (2003). No corrections were made for the Doppler shift caused

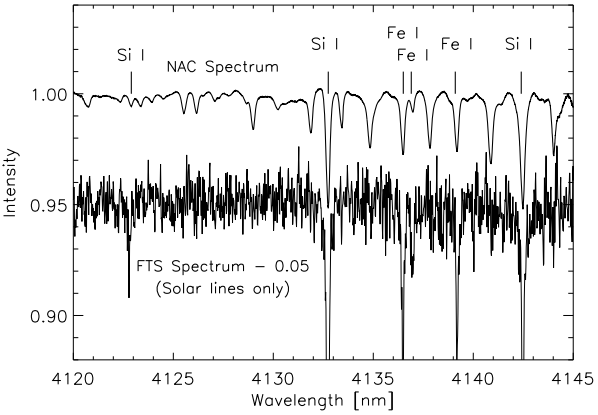

Figure 1 Intensity spectrum near 4135 nm. The top plot represents the NAC spectrum, the bottom plot is taken from the NSO McM/P *Fourier Transform Spectrometer* (FTS) from Wallace and Livingston (2003) offset by a small amount. The two Si I lines at 4132 and 4139 nm and the two Fe I lines at 4136 and 4137 nm are visible in absorption.

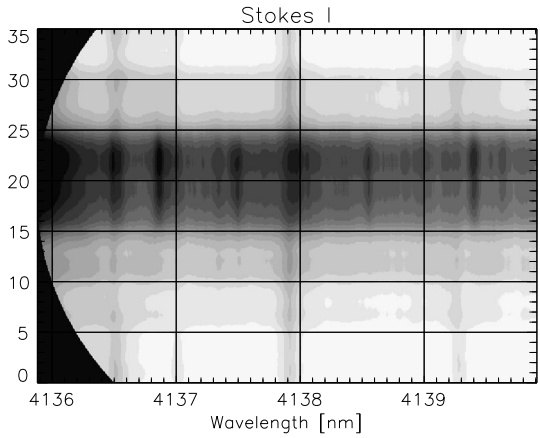

Figure 2 Intensity spectral frame from sunspot observations near 4135 nm. The sunspot in NOAA 11846 was observed on 25 September 2013 at solar-disk position $\mu = 0.76$. The penumbra covers spectral slit positions from 5 – 15 arcsec and 25 – 30 arcsec, the umbra is visible from 15 – 25 arcsec, and the rest of the slit covers the quiet Sun.

by the relative motion of the Sun and the telescope, nor for the gravitational redshift of the Sun. As shown in Table 1, the three Si I line centers were measured at positions of 4122.90, 4132.75, and 4142.48 nm, and the three Fe I line centers were measured to be at 4136.50, 4136.99, and 4139.19 nm. The uncertainty in these observed wavelengths is about ± 0.005 nm.

The observed line depths from the NAC observations correlate well with the line depths from ATMOS (Geller, 1992) with the exception of the 4142 nm Si I line. The NAC line depths are roughly one-third of the ATMOS line depths, except that in the NAC observations the 4142 nm line is about twice as deep as this relationship would suggest.

Figure 2 shows a spectral frame from the 25 September 2013 observations; in this frame, the upper and lower sections of the slit show the quiet-Sun spectrum, the middle of the slit crosses a sunspot umbra, and the other parts of the slit show signal from the penumbral regions. The spectral range covers from about 4136 to 4141 nm. This frame was produced by averaging the spectrum from 240 individual exposures after each was shifted to align the sunspot position along the slit. Residual seeing motions perpendicular to the slit were not corrected and so some spatial smearing is introduced. The umbral regions of this sunspot show a continuum brightness of about 0.72 times the quiet-Sun brightness. As shown in Figure 2, there are several spectral lines that are not present in the quiet-Sun regions, but appear in the sunspot umbral regions. They were identified using the results of Wallace,

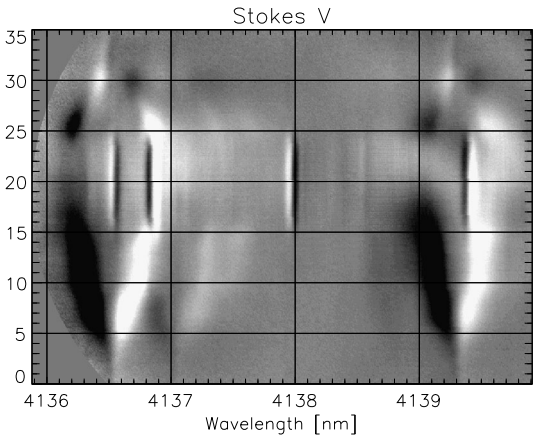

Figure 3 Stokes V spectral frame from sunspot observations near 4135 nm. The sunspot in NOAA 11846 was observed on 25 September 2013 at solar disk position $\mu = 0.76$. The penumbra covers spectral slit positions from 5 – 15 arcsec and 25 – 30 arcsec, the umbra is visible from 15 – 25 arcsec, and the rest of the slit covers the quiet Sun.

Hinkle, and Livingston (2002). The strongest molecular lines seen in the intensity spectrum are at the following measured wavelengths (all in nm): 4136.48 (OH or SiO), 4136.85 (SiO), 4137.48 (SiO or CO), 4137.98 (OH), 4138.54 (SiO), 4139.40 (OH), 4139.63 (SiO), and 4140.75 (SiO). In all cases the error in the line-center wavelength is estimated to be about ± 0.02 nm. The only ATMOS molecular identifications in this range listed in Geller (1992) are from OH at 4136.79 and 4139.26 nm; these lines are not seen in the sunspot spectra of Wallace, Hinkle, and Livingston (2002), nor in these NAC sunspot spectra.

4.2. The Polarization Spectra at 4135 – 4139 nm

The Stokes spectra of these lines show a wealth of details. In Figure 3, a Stokes V spectral frame is shown; this corresponds to the same position as the Stokes I frame shown in Figure 2. This and subsequent Stokes Q and Stokes U frames are made by analyzing 30 waveplate rotations, each of which was sampled with eight exposures. As in the Stokes I spectral frame, motion of the sunspot along the slit was corrected, but motion perpendicular to the slit will add spatial smearing, and possibly spectral broadening as slightly different magnetic fields are sampled in each exposure. It is important to note that all three spectral lines are affected in identical ways, since they all appear in the same spectral frame. This frame prominently shows the circular polarization signature from the three Fe I spectral lines, as well as the spectra from four molecular lines confined to the sunspot umbra.

The averaged spectral frame shown in Figure 3 reveals that the McM/P observations from the NAC currently lack the signal-to-noise ratio needed to measure the magnetic fields in the quiet Sun outside of the penumbra. The spectral lines sample the penumbral fields well, but when the field strength increases, some of the Zeeman components from 4136 and 4137 nm blend. The lines are very weak in the sunspot umbra, and do not seem useful for measuring the magnetic fields there.

To examine the relative magnetic splittings, the NAC Stokes V profiles were examined using a number of techniques. The analysis was restricted to spectral frames showing two or more lines; in this way, the spectral lines are identically affected by seeing conditions and the spectral lines sample identical solar magnetic fields. The splitting was examined by eye using spectral profiles; then the Stokes signals in several frames were examined by hand. Another more detailed analysis involved finding the wavelength positions of the Stokes V σ-spectral (circularly polarized) components at several slit positions and fitting a polynomial

Table 4 Zeeman line splittings relative to Fe I 4139 nm.

Atom	Wavelength [nm]	Kurucz ratio (*vs.* 4139 nm)	Measured ratio (*vs.* 4139 nm)
Si I	4132.7		1.00 ± 0.12 (3)
Fe I	4136.5	1.23	1.12 ± 0.67 (2)
			1.28 ± 0.14 (4)
			1.39 ± 0.07 (5)
			1.32 ± 0.03 (6)
Fe I	4137.0	2.13	1.84 ± 0.21 (6)

function to these splittings to derive the splittings along the whole slit. In most cases, both σ components were used for these measurements; however, when the components were blended or outside of the spectral frame, one component was measured relative to the line center position.

The measured splittings for all the lines were then compared to the splitting of the Fe I 4139 nm. The results are presented in Table 4. The sources of error to considered in these measurements are the uncertainty in the wavelength position of the σ component (small), the spatial scatter in the ratio of the splitting in well-measured penumbral regions (reported in Table 4), and the uncertainty in the line-center position in cases where only one σ component is measurable (difficult to quantify, but estimated to be small).

According to Stenflo (1994), the Zeeman splitting of a line is $\Delta\lambda = 4.6710^{-13} g_{\rm eff} \lambda^2 B$, where B is the solar magnetic field causing the splitting. Here we ignored the 0.2 % changes caused by the different wavelengths of the lines. As long as the magnetic field being measured is identical, we can compute the ratio of the $g_{\rm eff}$ values for each line as the ratio of the observed splittings $\frac{g_{4136}}{g_{4139}} = \frac{\Delta\lambda_{4136}}{\Delta\lambda_{4139}}$. The lines were measured at the same disk position on the Sun because they appear in the same spectral frame. We calculated formation heights for the 4132, 4136, and 4139 nm lines to be 200, 175, and 125 km above the continuum height. Assuming a vertical magnetic field gradient of 3 $\mathrm{G\,km^{-1}}$ and an assumed magnetic field strength of 2000 G, the magnetic field sampled by the 4132 nm line would be 0.89 weaker than the 4139 nm line, while the 4136 nm line would sample a field 0.92 weaker than the 4139 nm line. While the height of formation differences may explain the measurement error seen in the 4132 nm splitting ratio, they cannot explain the measured splitting ratio seen with 4136 nm. Currently we cannot compute the formation height of the weak 4137 nm line, and the role of a vertical magnetic gradient remains a mystery with the splitting ratio seen for that line.

The splitting for the Fe I 4137 nm line is a special case, since as revealed by Figure 3, the line seems to display multiple σ components in the Stokes V spectrum. The individual components are split by factors of 1.44 ± 0.05 and 2.55 ± 0.23, respectively. The amplitude ratio of the two components is difficult to measure, but is estimated to be 1.75 ± 0.25, with the component with the larger shift having the weaker Stokes V amplitude. Using the averaging technique described by Beckers (1969), the Landé factor for this line is then determined to be $g_{\rm eff} = 1.84 \pm 0.21$.

Four of the molecular lines seen in the sunspot from 25 September 2013 show strong Stokes V profiles. These are the lines at 4136.48 (OH or SiO), 4136.85 (SiO), 4137.98 (OH), and 4139.40 nm (OH). The lines at 4136.48 and 4137.98 nm show a Stokes V profiles that has the opposite sense of the atomic and the other molecular lines; these transitions have a negative $g_{\rm eff}$.

Table 5 Stokes V amplitudes relative to OH 4139.63 nm.

Molecule	Wavelength [nm]	$\partial I/\partial\lambda$ (*vs.* 4139.63 nm)	Stokes V (*vs.* 4139.63 nm)	$g_{\rm eff}$ ratio (*vs.* 4139.63 nm)
OH (or SiO)	4136.48	1.04	−0.8	−0.77
SiO	4136.85	0.98	1.25	1.28
OH	4137.98	1.05	−0.8	−0.77

None of the molecular lines show completely resolved splitting profiles in the sunspot umbra, instead, they resemble the types of unresolved Stokes V profiles seen in weak magnetic fields. Using the weak-field approximation, we can compare the relative $g_{\rm eff}$ of the lines by examining the amplitudes of the Stokes I derivatives and Stokes V profiles of the lines. According to Stenflo (1994), when the Zeeman splitting of a line is weaker than the Doppler broadening, the Stokes V signal can be approximated by $V(\lambda) \approx B g_{\rm eff} \frac{\partial I}{\partial \lambda}$, where B is the solar magnetic field causing the splitting. Again, as long as the magnetic field being measured is identical (a condition that is satisfied when the lines are in the same spectral image), then we can compute the ratio of the $g_{\rm eff}$ values for line 1 compared to line 2 as the ratio of $\frac{g_1}{g_2} = \frac{V_1}{V_2} \frac{\partial I_2/\partial\lambda}{\partial I_1/\partial\lambda}$. In Table 5 we list the ratios of the Stokes I derivatives and V amplitudes of the lines, normalizing all of the lines by the ratio of the OH line at 4139.63 nm. While the Stokes I derivatives for these lines are within a few percent of each other, there are larger differences in the Stokes V amplitudes. The measurement errors in these relative values are small, but the systematic errors caused by an uncertain background subtraction are estimated at the level of 10 %. In the two cases where the molecules show an inverted Stokes V profile, the ratio is listed as negative. From the values in the table it is clear that the SiO line at 4136.85 nm has the highest value for $g_{\rm eff}$ of all four of these lines.

The Stokes Q and U polarization profiles are very strange for the Fe I 4137 nm spectral line. Both the 4136 nm and 4139 nm Fe I lines show typical linear polarization profiles with central π components and magnetically shifted σ components. For both lines the σ components have the same polarity at a given spatial location in the penumbra. However, the 4137 nm line is different. First, there is no unshifted central π component in the Stokes Q or Stokes U profile. Second, the magnetically split σ components are visible, but they have the opposite polarity as the σ components for the 4136 and 4139 nm lines. This is unexpected, especially since the Stokes V profiles for all three Fe I lines show the same polarity for the magnetically shifted σ components. The molecular absorption lines in the sunspot umbra seem to show no signals in the linear polarization Stokes Q and Stokes U data.

5. Conclusions

The identification of the 4135 nm region of infrared solar spectral lines with particular transitions in Fe I and Si I is difficult, but the latest observations from the NSO McM/P using the NAC confirms several identifications made by Kurucz (2011). Relative to the Fe I line at 4139 nm, the Zeeman splitting of the 4136 nm line is 1.28 ± 0.17, consistent with the prediction from the intermediate coupling model. The Zeeman splitting of the Fe I line at 4137 nm shows two components, with an intensity-averaged splitting of about twice the 4139 nm line splitting; this is roughly consistent with the value predicted from the intermediate coupling. The magnetic sensitivity of this line is therefore very high, with a $\lambda g_{\rm eff} = 11\,600$. While these lines may be useful for sunspot penumbra observations, their main advantage will be

realized with future observations with lower backgrounds, where they will be a critically useful diagnostic of quiet-Sun magnetic fields.

Acknowledgements We wish to thank Robert Kurucz for clarifying discussions and the anonymous referee for a thorough review. NSO is operated by AURA Inc., under contract to the National Science Foundation. PG acknowledges AFOSR grant FA9550-15-1-0322.

Disclosure of Potential Conflicts of Interest The authors declare that they have no conflicts of interest.

References

Beckers, J.M.: 1969, *A table of Zeeman multiplets*. Sac. Peak Obs. Contr. 141. ADS.

Cao, W., Gorceix, N., Coulter, R., Ahn, K., Rimmele, T.R., Goode, P.R.: 2010, Scientific instrumentation for the 1.6 m New Solar Telescope in Big Bear. *Astron. Nachr.* **331**, 636. ADS. DOI.

Curtis, L.J.: 2003, *Atomic Structure and Lifetimes: A Conceptual Approach*, Cambridge Univesity Press, Cambridge, 161. ADS.

Farmer, C.B., Norton, R.H.: 1989, *A High-Resolution Atlas of the Infrared Spectrum of the Sun and the Earth Atmosphere from Space. A Compilation of ATMOS Spectra of the Region from 650 to* 4800 cm^{-1} *(2.3 to 16 μm). Vol. I. The Sun*, NASA, Washington. ADS.

Geller, M.: 1992, *A High-Resolution Atlas of the Infrared Spectrum of the Sun and the Earth Atmosphere from Space. Vol. III. Key to Identification of Solar Features*, NASA, Washington.

Geller, M.: 1995, Line identification in ATMOS solar spectra. In: Sauval, A.J., Blomme, R., Grevesse, N. (eds.) *Laboratory and Astronomical High Resolution Spectra*, *Astron. Soc. Pacific* **CS-81**, 88. ADS.

Johansson, S., Cowley, C.R.: 1988, Complex atoms in astrophysical spectra. *J. Opt. Soc. Am. B, Opt. Phys.* **5**, 2264. ADS. DOI.

Kurucz, R.L.: 2011, Including all the lines. *Can. J. Phys.* **89**, 417. ADS. DOI.

Lin, H.: 2003, ATST near-IR spectropolarimeter. In: Keil, S.L., Avakyan, S.V. (eds.) *Innovative Telescopes and Instrumentation for Solar Astrophysics*, *SPIE CS* **4853**, 215. ADS.

Martin, W., Zalubas, R.: 1983, Energy levels of silicon, Si I through Si XIV. *J. Phys. Chem. Ref. Data* **12**, 323.

Nave, G., Johansson, S., Learner, R.C.M., Thorne, A.P., Brault, J.W.: 1994, A new multiplet table for Fe I. *Astrophys. J. Suppl.* **94**, 221. ADS. DOI.

Pierce, A.K.: 1964, The McMath solar telescope of Kitt Peak National Observatory. *Appl. Opt.* **3**, 1337. ADS. DOI.

Rabin, D., Jaksha, D., Kopp, G., Mahaffey, C.: 1992, NIM – a Near Infrared Magnetograph. *Bull. Am. Astron. Soc.* **24**, 1251. ADS.

Stenflo, J.: 1994, *Solar Magnetic Fields: Polarized Radiation Diagnostics*, *Astrophys. Space Scien. Lib.* **189**, Kluwer Academic, Dordrecht. ADS.

Sugar, J., Corliss, C.: 1985, *Atomic Energy Levels of the Iron-Period Elements: Potassium Through Nickel*, Am. Chem. Soc., Washington. ADS.

Wallace, L., Livingston, W.: 2003, *An Atlas of the Solar Spectrum in the Infrared from 1850 to* 9000 cm^{-1} *(1.1 to 5.4 Micrometer)*. NSO Technical Report. ADS.

Wallace, L., Livingston, W.C.: 1992, *An Atlas of a Dark Sunspot Umbral Spectrum from 1970 to* 8640 cm^{-1} *(1.16 to 5.1 [Microns])*. NSO Technical Report 92-001. ADS.

Wallace, L., Hinkle, K., Livingston, W.C.: 2002, *Sunspot Umbral Spectra in the Regions 1925 to 2226 and 2392 to* 3480 cm^{-1} *(2.87 to 4.18 and 4.48 to 5.35 [Microns])*. NSO Technical Report 02-001. ADS.